A Commander-independent function of COMMD3 in endosomal trafficking

Galen T. Squiers[1], Chun Wan[1], James Gorder[1], Harrison Puscher[1#], Jingshi Shen[1*]

[1]Department of Molecular, Cellular and Developmental Biology, University of Colorado, Boulder, CO 80309, USA.

[#]Present address: Department of Biological Sciences, University of Southern California, Los Angeles, CA 90089, USA.

[*]Correspondence to: jingshi.shen@colorado.edu

Keywords: endocytic pathway, membrane trafficking, endosome, Golgi, Commander, Retromer, plasma membrane, endosomal recycling.

ABSTRACT

Endosomal recycling is a branch of intracellular membrane trafficking that retrieves endocytosed cargo proteins from early and late endosomes to prevent their degradation in lysosomes. A key player in endosomal recycling is the Commander complex, a 16-subunit protein assembly that cooperates with other endosomal factors to recruit cargo proteins and facilitate the formation of tubulo-vesicular carriers. While the crucial role of Commander in endosomal recycling is well established, its molecular mechanism remains poorly understood. Here, we genetically dissected the Commander complex using unbiased genetic screens and comparative targeted mutations. Unexpectedly, our findings revealed a Commander-independent function for COMMD3, a subunit of the Commander complex, in endosomal recycling. COMMD3 regulates a subset of cargo proteins independently of the other Commander subunits. The Commander-independent function of COMMD3 is mediated by its N-terminal domain (NTD), which binds and stabilizes ADP-ribosylation factor 1 (ARF1), a small GTPase regulating endosomal recycling. Mutations disrupting the COMMD3-ARF1 interaction diminish ARF1 expression and impair COMMD3-dependent cargo recycling. These data provide direct evidence that Commander subunits can function outside the holo-complex and raise the intriguing possibility that components of other membrane trafficking complexes may also possess functions beyond their respective complexes.

INTRODUCTION

Proteins embedded in the plasma membrane transduce signals, import nutrients, and sense physical changes, enabling cells to respond to external cues [1-3]. The cell has evolved complex and interconnected mechanisms to maintain membrane protein levels on the cell surface and to adjust these levels in response to stimuli [1, 4]. Disruption of membrane protein homeostasis underlies many human diseases, including cancer, metabolic disorders, and neurodegeneration [5-7]. Surface levels of a membrane protein are established through exocytosis, a vesicle fusion event, and internalization via endocytosis, a vesicle budding process [1, 8, 9]. In addition to exocytosis and endocytosis, another branch of intracellular membrane trafficking – endosomal recycling – also plays a crucial role in maintaining surface protein homeostasis [10-14]. Following endocytosis, endocytic vesicles fuse into early endosomes, which then progress into late endosomes [11, 15]. Within these endosomes, the cell determines which cargoes proceed to lysosomal degradation and which are rescued from degradation through recycling [10-13]. Cargoes retrieved from endosomes are packaged into tubulo-vesicular transport carriers and are either recycled back to the plasma membrane or routed to the *trans*-Golgi network (TGN) for re-entry into the exocytic pathway [10-13].

Two central players in endosomal retrieval are Retromer and Commander. Retromer, a heterotrimeric complex comprised of VPS35, VPS29, and VPS26, recruits cargo proteins on the endosome and mediates the formation of tubulo-vesicular carriers for retrograde trafficking to the TGN or recycling to the plasma membrane [13, 16-18]. The Commander complex, which primarily sorts cargoes from endosomal compartments to the plasma membrane, is a large protein complex composed of the Retriever subcomplex and the CCC subcomplex (COMMD-CCDC22-CCDC93) (Fig. 1A) [6, 7, 12, 19-22]. The Retriever subcomplex is a heterotrimer consisting of

VPS35L/C16ORF62, VPS26C/DSCR3, and VPS29, and shares a similar overall configuration with Retromer [22]. The CCC complex includes 10 COMMD proteins (COMMD1-10), which interact through their conserved C-terminal copper metabolism MURR1 domains (COMMDs) [23-25]. The COMMD proteins bind CCDC22 and CCDC93 to form the CCC subcomplex, which also contains DENND10 [6, 20]. The 13-subunit CCC subcomplex combines with the Retriever subcomplex to form the 16-subunit Commander holo-complex (Fig. 1A) [6, 7, 19]. On the endosome, Retromer and Commander cooperate with other factors such as sorting nexins (SNXs), Rab GTPases, actin, and the actin-remodeling WASH complex to capture cargoes and facilitate the formation of tubulo-vesicular carriers [10, 12, 20, 26].

The Commander complex is ubiquitously expressed, and its 16 subunits display a stringent equimolar stoichiometry within the holo-complex [6, 7, 19, 27], supporting the notion that these subunits function collectively in endosomal recycling. However, Commander subunits exhibit distinct tissue-specific expression patterns and can associate with different sets of proteins [19, 23, 25, 28]. Furthermore, CCC and Retriever also exist as subcomplexes, whereas COMMD proteins are found in pools of homo- and hetero-oligomers independent of the Commander complex [6, 7, 23, 29]. These observations have led to the hypothesis that Commander subunits may have functions beyond their role in the Commander holo-complex [30-33]. However, direct evidence for this hypothesis is still lacking.

In this work, we systematically dissected the Commander complex through unbiased genetic screens and comparative targeted mutations. Interestingly, we discovered that COMMD3, a subunit of the Commander complex, functions in endosomal recycling independently of other Commander subunits, in addition to its Commander-dependent activity. Comparative genetic analyses revealed that COMMD3 regulates a group of cargo proteins that do not require the

Commander holo-complex. This Commander-independent function is mediated by the N-terminal domain (NTD) of COMMD3, which binds and stabilizes ADP-ribosylation factor 1 (ARF1). Guided by an AlphaFold-predicted structural model, we introduced point mutations into COMMD3 to disrupt its binding to ARF1. We found that these mutations diminish ARF1 expression and impair the Commander-independent function of COMMD3. Together, these findings uncovered a role of COMMD3 in endosomal trafficking independent of the Commander holo-complex, and suggest that other membrane trafficking complexes may also possess functions beyond their canonical roles within their respective complexes.

RESULTS

Genetic analysis of the Retromer and Commander complexes using unbiased genome-wide CRISPR screens

Unbiased genome-wide genetic screens are a powerful approach to study the functions of membrane trafficking genes in cultured mammalian cells [8, 9, 34]. Previously, we conducted an genome-wide CRISPR screen to identify new regulators of surface protein homeostasis using a surface protein reporter (GLUT-SPR) based on the glucose transporter GLUT4 [8]. Mouse preadipocytes expressing the GLUT-SPR reporter were mutagenized using the genome-wide GeCKO v2 CRISPR library [35]. In the genome-wide CRISPR screen, we used fluorescence-activated cell sorting (FACS) to isolate mutant preadipocytes with reduced surface levels of the GLUT-SPR reporter [8]. The screen recovered known regulators of cargo exocytosis and enabled us to identify previously uncharacterized exocytic regulators, including Reps1 and Ralbp1 [8]. Importantly, the new exocytic regulators identified in this GLUT-SPR-based CRISPR screen broadly regulate the surface proteostasis of membrane proteins [8].

To gain new insights into the molecular functions of Retromer and Commander, we re-analyzed the data from the CRISPR screen to examine genes encoding Retromer and Commander subunits. The CRISPR library used in the screen contained guide RNAs (gRNAs) targeting the genes encoding the subunits of the Retromer and Commander complexes (Fig. 1A-B). The GLUT-SPR-based CRISPR screen isolated *Vps35* and *Vps29* (Fig. 1C), which encode subunits of the Retromer complex, consistent with the critical role of Retromer in the endosomal recycling of GLUT4 [34, 36]. Genes encoding Vps26 were not recovered in the screen due to redundancy (*Vps26a* and *Vps26b*). Recovery of the Retromer genes also suggests that the CRISPR screen has the sensitivity and specificity to systematically examine the functional roles of endosomal

recycling genes. Genes encoding the unique subunits of the Retriever complex – *Vps35l* and *Vps26c* – were not isolated in the CRISPR screen (Fig. 1C). Similarly, virtually none of the genes encoding the CCC complex were recovered as significant hits in the CRISPR screen, except for *Commd3*, which encodes the COMMD3 subunit of the Commander complex (Fig. 1A-C) [6]. These data indicate that the Commander complex is dispensable for the endosomal recycling of GLUT-SPR.

To further characterize the functional roles of Retromer- and Commander-encoding genes in cell physiology, next we examined whether these genes are essential for cell viability or growth by re-analyzing data from an unbiased genome-wide essentiality screen. In the essentiality screen, mouse preadipocytes mutagenized by the CRISPR GeCKO v2 library were continuously passaged for two weeks without any selection [8]. The abundance of gRNAs in this cell population was sequenced and compared with that in the original CRISPR gRNA library. If a gene is essential for cell viability or growth, its corresponding gRNAs would be depleted after the two-week cell passage. We found that none of the genes encoding the Retromer and Commander complexes are essential in mouse preadipocytes (Fig. 1D). Thus, the disruption of either the Retromer or Commander-dependent endosomal retrieval pathways does not impair the viability or proliferation of these cells.

Together, these global genetic analyses suggest that COMMD3 plays an unrecognized role in GLUT-SPR trafficking, independent of its canonical function within the Commander holo-complex.

Deletion of COMMD3 disrupts endosomal trafficking

To validate the role of COMMD3 in the surface homeostasis of GLUT-SPR, we deleted the *Commd3* gene in mouse preadipocytes (Fig. 2A). Indeed, surface levels of GLUT-SPR were strongly reduced in *Commd3* KO preadipocytes, which were either cultured under standard conditions or stimulated with insulin to mimic a physiological fed state (Fig. 2B). These data confirm the findings from the CRISPR screen (Fig. 1C). To examine whether COMMD3 regulates the surface homeostasis of GLUT-SPR in another cell type, the fibroblast-like preadipocytes were differentiated into mature adipocytes, which are morphologically and functionally distinct from preadipocytes [37]. Using flow cytometry, we observed that surface GLUT-SPR levels were markedly reduced in *Commd3* KO adipocytes (Fig. 2C), indicating that the role of COMMD3 in surface protein homeostasis is not restricted to a single cell type. Similar findings were observed in adipocytes using confocal imaging (Fig. 2D). Surface levels of GLUT-SPR were substantially decreased in *Commd3* KO cells, concomitant with elevated intracellular accumulation of the reporter (Fig. 2D). These results demonstrated a critical role of COMMD3 in the endosomal trafficking of GLUT-SPR.

To further characterize the function of COMMD3 in the endosomal trafficking of GLUT-SPR, we stained for EEA1, an early endosome marker [38], and examined the morphology of EEA1-positive organelles. We observed that the morphology of EEA1-positive endosomes was significantly altered in *Commd3* KO cells (Fig. 3A). The size of the EEA1-positive endosomes markedly increased in *Commd3* KO cells (Figs. 3A-B). We also observed elevated GLUT-SPR accumulation in EEA1-positive endosomes in *Commd3* KO cells (Fig. 3C). Next, we used Structured Illumination Microscopy (SIM) to visualize the localization of GLUT-SPR and Rab5, another marker of the early endosome [39]. We found that a portion of GLUT-SPR resided in Rab5-

positive compartments and its co-localization with Rab5 increased in *Commd3* KO cells (Fig. 3D-E).

Together, these data demonstrate that deletion of *Commd3* leads to the enlargement of early endosomes and accumulation of GLUT-SPR in these compartments, consistent with a trafficking defect occurring at the endosomal recycling step.

COMMD3 regulates endosomal trafficking in a Commander-independent manner

Next, we sought to confirm the Commander-independent function of COMMD3 using comparative targeted mutations. We deleted genes encoding other Commander subunits and compared the phenotypes of the KO cells with that of *Commd3* KO cells. The COMMD proteins are found in three subcomplexes prior to forming the heterodecameric COMMD complex: subcomplex A (COMMD1-4-6-8), subcomplex B (COMMD2-3-4-8), and subcomplex C (COMMD5-7-9-10) [6]. Here, we selected COMMD1, COMMD3 and COMMD5 as representative subunits of the three subcomplexes. We measured surface levels of integrin alpha-6 (ITGA6), a known Commander-dependent cargo [22], in cells lacking one of the COMMD proteins. As expected, surface levels of ITGA6 were downregulated in all these KO cell lines (Fig. 4A), confirming the canonical role of COMMD3 within the Commander holo-complex.

Next, we examined the trafficking of other cargo proteins. Corroborating the results of the CRISPR screen, we found that surface levels of GLUT-SPR remained unchanged in the *Commd1* KO cells and were only slightly affected in *Commd5* KO cells, in contrast to the strong reduction observed in *Commd3* KO cells (Fig. 4B). Surface levels of the transferrin receptor (TfR), a Commander-independent cargo [40], were markedly decreased in *Commd3* KO cells but remained intact in *Commd1* or *Commd5* KO populations (Fig. 4C). Surface levels of lysosomal-associated

membrane protein 1 (LAMP1) were also strongly decreased in *Commd3* KO cells but were not substantially changed in *Commd1* or *Commd5* KO cells (Fig. 4D). Together, comparative analysis of these diverse membrane proteins clearly demonstrates that COMMD3 regulates a group of cargo proteins independent of the Commander holo-complex, in addition to its canonical function within the Commander complex.

Mutations of CCDC93 or Retriever lead to upregulation of COMMD3

To further characterize the Commander-independent function of COMMD3, we examined the KO phenotypes of other Commander subunits. We observed that the expression of CCDC93 and VPS35L was substantially decreased in *Commd3* KO cells, and VPS35L expression was diminished in *Ccdc93* KO cells. These findings are consistent with the notion that stability of subunits within a protein complex is interdependent [8, 9]. Interestingly, we observed that COMMD3 expression was not reduced but upregulated in *Ccdc93* or *Vps35l* KO cells (Fig. 5A). Thus, unlike other Commander subunits, COMMD3 persists when other subunits of the Commander complex are depleted, further supporting the ability of COMMD3 to regulate endosomal trafficking independent of the Commander holo-complex.

The upregulation of COMMD3 in Commander-deficient cells, which likely reflects a compensatory mechanism, offers another strategy to test the Commander-independent function of COMMD3. We reasoned that if a cargo is dependent on COMMD3 but not on the Commander complex, its surface levels could be increased in cells with elevated COMMD3. Indeed, we observed that surface levels of TfR, a cargo dependent on Commd3 but not on the Commander complex (Fig. 4C) [40], were markedly increased in *Ccdc93* or *Vps35l* KO cells (Fig. 5B). Conversely, surface TfR levels were diminished in *Commd3* KO cells and were fully restored by

expression of a *Commd3* rescue gene (Fig. 5B). KO of both *Commd3* and *Ccdc93* resulted in decreased surface levels of TfR (Fig. 5C), confirming that the elevated surface TfR observed in *Ccdc93* KO cells was caused by COMMD3 upregulation. Consistent with this notion, overexpression of *Commd3* in WT cells markedly elevated TfR surface levels (Fig. 5D). Altogether, these results demonstrate that COMMD3 is upregulated in Retriever- or CCDC93-deficient cells and enhances the endosomal retrieval of COMMD3-dependent cargoes, further supporting a Commander-independent role of COMMD3 in endosomal recycling.

The NTD of COMMD3 mediates its commander-independent function and interacts with ARF1

Next, we sought to determine the molecular mechanism by which COMMD3 regulates endosomal trafficking in a Commander-independent manner. The COMMD3 protein is comprised of two autonomously folded domains – NTD and CTD (Fig. 6A). The C-terminal COMMD domains of COMMD proteins are well-conserved and mediate the formation of the heterodecameric COMMD complex within the Commander holo-complex [7, 41]. The NTDs of COMMD proteins share a similar structure but are more divergent in sequence [19, 29]. The function of the COMMD NTDs is unknown. Next, we examined whether the Commander-independent function of COMMD3 relies on its NTD. We expressed the COMMD3 NTD in *Commd3* KO cells and examined whether the KO phenotype could be rescued. Indeed, expression of the COMMD3 NTD fully restored the surface levels of TfR in *Commd3* KO cells (Fig. 6B), indicating that the NTD is sufficient for this function.

To gain molecular insights into the NTD of COMMD3, we determined the interactomes of full-length (FL) COMMD3, NTD, and C-terminal domain (CTD) (Fig. 6C-D). FL COMMD3,

NTD, and CTD were individually expressed and isolated through co-immunoprecipitation (co-IP), and the associated proteins within these samples were identified using mass spectrometry. Through this proteomic analysis, we identified a group of proteins present in the interactomes of FL COMMD3 and NTD but absent from the CTD interactome (Fig. 6E and Table S1). Among these proteins, ARF1 emerged as a strong candidate because it acts as a membrane trafficking regulator known to function on endosomes (Fig. 6F) [42, 43]. The ARF family of proteins are small GTPases involved in the recruitment of coat proteins, activation of membrane lipid-modifying enzymes, and interaction with the cytoskeleton [43, 44]. Using co-IP, we observed that the NTD of COMMD3 interacted with ARF1 (Fig. 6G), confirming the results of the proteomic experiments. Together, these data demonstrate that the NTD of COMMD3 mediates its Commander-independent function and interacts with ARF1.

COMMD3 regulates the stability of ARF1

To further characterize the interaction between COMMD3 and ARF1, we used SIM to visualize their subcellular localization. We observed significant co-localization between ARF1 and the NTD of COMMD3 (Fig. 7A-B), consistent with their interactions detected in proteomic and co-IP experiments (Fig. 6). We noted that, in the co-IP assays using 293T cells, ARF1 expression levels were significantly elevated when co-expressed with the NTD of COMMD3 (Fig. 6G). A similar ARF1-stabilizing effect was also observed in HeLa cells (Fig. 7C). These findings raised the possibility that COMMD3 uses its NTD to bind and stabilize ARF1. To test this model, we examined endogenous ARF1 levels in *Commd3* KO cells. Interestingly, we found that ARF1 levels were markedly reduced in *Commd3* KO cells and were fully restored upon introduction of a *COMMD3* rescue gene (Fig. 7D). To further investigate the functional link between COMMD3

and ARF1, we overexpressed ARF1 in *Commd3* KO cells. Strikingly, ARF1 overexpression fully restored the surface levels of TfR in *Commd3* KO cells (Fig. 7E). These data demonstrate that COMMD3 regulates endosomal trafficking through binding and stabilizing ARF1.

Mutations disrupting the COMMD3-ARF1 interaction impair the Commander-independent function of COMMD3

Finally, we sought to determine whether ARF1 binding is required for the Commander-independent function of COMMD3. AlphaFold3 predicted a high-confidence structure of the ARF1-GTP:COMMD3-NTD heterodimeric complex (Fig. 8A-B and Supplementary Dataset 1). According to this structural model, the α1 helix of COMMD3-NTD binds to the switch 1 of ARF1, while the α3 and α4 helices of COMMD3-NTD interact with the switch 2 of ARF1 (Fig. 8A-B and Supplementary Dataset 1). The switches 1 and 2 of ARF1 are highly conserved regions that are regulated by GTP binding and interact with effectors involved in endosomal recycling [45, 46]. The binding of COMMD3 to ARF1 is mainly mediated by hydrophobic interactions and hydrogen bonds, including hydrogen bonds formed by K60 and H61 of COMMD3 with Y81 of ARF1, K60 of COMMD3 with R79 and Q83 of ARF1, H63 of COMMD3 with H80 of ARF1 (Fig. 8A-B and Supplementary Dataset 1). AphaFold3 did not predict high-confidence structural models between COMMD3-NTD and ARF1-GDP or apo-ARF1, suggesting that COMMD3 selectively recognizes the GTP-bound form of ARF1. This conclusion is consistent with the observation that COMMD3 strongly stabilizes GTP-bound ARF1 (Figs. 6G and 7C)

Next, we introduced point mutations into the NTD of COMMD3 based on the structural model, aiming to disrupt its interaction with ARF1 (Fig. 8C). The COMMD3-NTD mutant was expressed at a similar level as the WT protein in *Commd3* KO cells (Fig. 8D). We observed that

the COMMD3-NTD mutant failed to restore surface levels of TfR, whereas WT COMMD3-NTD fully rescued the KO phenotype (Fig. 8E). In agreement with this finding, WT COMMD3-NTD, but not the mutant, restored ARF1 expression in *Commd3* KO cells (Fig. 8F). Altogether, these results further support the conclusion that COMMD3 regulates endosomal trafficking through binding and stabilizing ARF1.

DISCUSSION

The genetic evidence for a Commander-independent function of COMMD3 in endosomal trafficking is threefold. First, COMMD3 was the only Commander subunit isolated as a significant hit in a genome-scale genetic screen dissecting the surface homeostasis of GLUT-SPR, revealing a unique role of COMMD3 among Commander subunits in the GLUT-SPR trafficking pathway. Unbiased genetic screens are particularly powerful in dissecting a protein complex because they systematically interrogate the functional roles of all subunits within the complex [8, 9, 34, 47, 48]. Second, our comparative targeted mutations confirmed that the loss-of-function phenotype of COMMD3 is fundamentally distinct from that of other COMMD proteins. Besides GLUT-SPR, a group of other cargoes including TfR also selectively rely on COMMD3 but not on COMMD1 or COMMD5, further supporting the unique role of COMMD3 in the trafficking of these cargo proteins. It should be noted that our findings of ITGA6 are fully consistent with a canonical function of COMMD3 within the Commander holo-complex in endosomal recycling. Third, while the stability of Commander subunits is generally interdependent, COMMD3 persists when other subunits of the Commander complex are depleted. In fact, COMMD3 is upregulated when CCDC93 or Retriever are mutated, resulting in elevated surface levels of TfR.

The Commander-independent function of COMMD3 is mediated by its NTD, a domain previously lacking an ascribed function, whereas its C-terminal COMMD domain is required for the canonical role of COMMD3 within the Commander complex [6, 7, 19]. At the molecular level, the NTD of COMMD3 binds and stabilizes ARF1, a member of the ARF small GTPase family playing a key role in endosomal recycling [42, 49]. These findings suggest that GTP-ARF1 is intrinsically unstable prior to engaging its effectors and therefore requires stabilization by COMMD3. Since COMMD3 binds to the same regions of ARF1 recognized by ARF1 effectors, it

must dissociate from ARF1 before the latter can engage its effectors to regulate endosomal recycling [43]. Further research is needed to determine whether COMMD3 is released from ARF1 through direct competition by ARF1 effectors or if a more active mechanism is involved.

While unstable as monomers, COMMD proteins can exist as homo- or hetero-oligomers outside the Commander complex [30, 31, 50]. Since other COMMD proteins were not isolated as significant hits in our GLUT-SPR-based CRISPR screen, COMMD3 may form homo-oligomers before associating with ARF1 to regulate cargo trafficking in a Commander-dependent manner. The Commander-independent function of COMMD3 offers an additional route of endosomal recycling, alongside the Retromer- and Commander-dependent recycling pathways. By leveraging existing proteins such as COMMD3, the cell expands the repertoire of endosomal recycling routes without increasing gene numbers, which helps meet the formidable challenge of sorting thousands of membrane proteins that are constantly endocytosed into the cell. An important future direction is to determine precisely how COMMD3 interacts with ARF1 and how they cooperate with other endosomal regulators, such as SNXs, Rab GTPases, and the cytoskeleton to regulate cargo sorting on the endosome.

Our findings raise the intriguing possibility that other COMMD proteins may also possess additional functions outside the Commander holo-complex. In addition to endosomal recycling, Commander is also implicated in biological pathways including vesicle fusion, cytoskeletal organization, intracellular signaling, protein degradation, and gene expression [14, 22, 23, 30-33, 50-65]. Although many of these pathways are expected to require the Commander holo-complex, others may be mediated by stable pools of individual COMMD proteins outside the Commander complex. These Commander-dependent functions of COMMD proteins are supported by their evolutionary history. COMMD proteins evolved later than other Commander components,

concurrent with the expansion of genes encoding membrane trafficking regulators [66]. It is possible that precursors of COMMD proteins may have been stable and functional prior to joining the more ancient Commander core complex. As the Commander holo-complex emerged, some of the primordial functions of COMMD precursors were likely retained in COMMD proteins. Further evidence supporting Commander-independent functions is the distinct tissue-specific expression patterns of COMMD proteins [19, 23, 25, 28, 67]. Given their differential expression, a portion of COMMD proteins inevitably exists outside the Commander holo-complex and may play cell type-specific physiological roles. Besides Commander, other membrane trafficking complexes might also contain subunits functioning outside the homo-complexes. In line with this notion, SEC13, a component of the COPII coat formed on the endoplasmic reticulum (ER), is also implicated in the formation of the nuclear pore complex (NPC) [68, 69]. We suggest that the genetic strategy described in this study will be instrumental in determining whether and how COMMD proteins and SEC13 regulate cell physiology independently of their respective holo-complexes.

EXPERIMENTAL PROCEDURES

Cell culture

Mouse preadipocytes, HeLa cells, and 293T cells were cultured in Dulbecco's Modified Eagle Medium (DMEM) supplemented with 10% FB Essence (FBE, VWR, #10803-034) and penicillin/streptomycin (Thermo Scientific, #15140122). All cell lines were maintained in a humidified incubator at 37 °C with 5% CO_2. To differentiate preadipocytes into mature adipocytes, preadipocytes were grown to ~95% confluence before a differentiation cocktail was added at the following final concentrations: 5 µg/mL insulin (Sigma, #I0516), 1 nM Triiodo-L-thyronine (T3, Sigma, #T2877), 125 µM indomethacin (Sigma, #I-7378), 5 µM dexamethasone (Sigma, #D1756), and 0.5 mM 3-isobutyl-1-methylxanthine (IBMX, Sigma, #I5879). After two days, the cells were switched to DMEM supplemented with 10% FBE, 5 µg/mL insulin, and 1 nM T3. After another two days, fresh DMEM media supplemented with 10% FBE and 1 nM T3 were added to the cells. Differentiated adipocytes were usually analyzed six days after addition of the differentiation cocktail.

Gene KO using CRISPR-Cas9

Genome-wide CRISPR screens of GLUT-SPR surface homeostasis and gene essentiality were described previously [8]. To individually ablate a candidate gene, gRNAs targeting the gene were chosen via the CRISPick algorithm (https://portals.broadinstitute.org/gppx/crispick/public) to maximize KO efficiency and minimize off-target effects. The upstream guide was cloned into the pLenti-CRISPR-v2 vector (Addgene, #52961) and the downstream guide was cloned into a modified version of the pLentiGuide-Puro vector (Addgene, #52963), in which the puromycin selection marker was replaced with a hygromycin selection marker.

Guide sequences targeting the mouse *Commd3* gene are: CTTCGCGCTTCTCCTCCGGG and CTTGAAACAGATCGACCCAG. Guide sequences targeting the mouse *Commd1* gene are: TCACGGACACTCGGGTGTCA and ACTGCTCAAACCAAAAAGCA. Guide sequences targeting the mouse *Commd5* gene are: GTTGTTGAAACTCGTAGTCG and TGCCAGCGCCAACCTGTCAG. Guide sequences targeting the mouse *Ccdc93* gene are: CGAAAGTACCGACGGCAGCG and GATGACCGCCATGGCAAACG. Guide sequences targeting the mouse *Vps35l* gene are: GGATTATGTGAACCGCATAG and GGAGGTTTGCAAGTGCATCA. Double KO cells of *Commd3* and *Ccdc93* were generated using one guide per gene: *Commd3* – CTTCGCGCTTCTCCTCCGGG and *Ccdc93* – GATGACCGCCATGGCAAACG.

CRISPR plasmids were transfected into HEK 293T cells along with pAdVAntage (Promega, #E1711), pCMV-VSVG (Addgene, #8454), and psPax2 (Addgene, #12260). The 293T cell culture media containing lentiviral particles were harvested daily for four days and centrifuged at 25,000 rpm (113,000 g) for 1.5 hours at 4 °C using a Beckman SW28 rotor. Viral pellets were resuspended in PBS and used to infect target cells. After lentiviral infection, cells were selected using 3.5 µg/mL puromycin (Sigma, #3101118) for two days, followed by selection using 500 µg/mL hygromycin B (Thermo, #10687010) for another two days. All KO cells used in this work were pooled KO cell populations.

Gene expression in mammalian cells

The codon-optimized human *COMMD3* gene with a 3xFLAG-encoding sequence or an mCherry-3xFlag-encoding sequence was subcloned into the SHC003BSD-GFPD vector (Addgene, #133301). This *COMMD3* gene was not targeted by gRNAs used in the KO experiments. The

plasmid expressing the NTD (amino acids 1-124) of human COMMD3 was generated in a similar way. For the IP experiments, DNA fragments encoding FL and truncated human COMMD3 were subcloned into the SHC003BSD-GFPD vector. FL COMMD3 (amino acids 1-195) and NTD were fused to mCherry and 3xFlag tags at their C-termini. The CTD (amino acids 125-195) was fused to an mCherry tag at its N-terminus and a 3xFlag tag at its C-terminus. The human *ARF1* gene was subcloned into the SHC003BSD-GFPD vector with an HA-encoding sequence at the 3' end. The constructs were transfected into 293T cells to produce lentiviral particles using a similar procedure as CRISPR lentiviral production. The lentiviruses were used to infect target cells, followed by selection using 10 µg/mL blasticidin (Thermo Fisher Scientific, #BP2647).

Flow cytometry

Cells grown on cell culture plates were washed with ice-cold KRH buffer and blocked at 4°C with KRH buffer supplemented with 5% FBE. Subsequently, the cells were labeled for one hour with KRH buffer containing 2% FBE and the following antibodies: anti-HA (BioLegend, #901501, RRID: AB_2565006), APC-conjugated anti-LAMP1 (BioLegend, #328619, RRID:AB_1279055), anti-ITGA6 (Invitrogen, #14-0495-82, RRID:AB_891480), APC-conjugated anti-mouse secondary antibodies (eBioscience, #17-4015-82, RRID: AB_2573205), APC conjugated anti-rat antibodies (Invitrogen, #A10540, RRID:AB_10562535), and APC-conjugated anti-TfR/CD71 antibodies (BioLegend, #334108, RRID:AB_10915138). Following antibody labeling, cells were washed twice with KRH buffer containing 5% FBE, and once with PBS. Cells were dissociated using Accutase before resuspension in PBS buffer containing 5% FBE. Cells were analyzed in triplicate on a CyAN ADP analyzer (Beckman Coulter). To calculate surface levels of GLUT-SPR, mean APC values were divided by mean GFP fluorescence.

Immunostaining and imaging

Cells grown on glass coverslips were washed with PBS and fixed using 4% PFA in PBS. Cells were then permeabilized using 0.1% Tween-20 and blocked with PBS buffer containing 5% FBE. Permeabilization was omitted when surface proteins were stained. Cells were labeled for one hour with 2% FBE in PBS using the following antibodies: anti-HA, anti-FLAG M2 (Sigma-Aldrich, #F1804, RRID: AB_262044), Alexa Fluor 647-conjugated anti-mouse IgG (Invitrogen, #A32733, RRID: AB_2633282), and Alexa Fluor 568-conjugated anti-rabbit IgG (Thermo Fisher Scientific, #A11004, RRID: AB_2534072). Confocal images were acquired on a Nikon A1 laser scanning confocal microscope using a 100× oil immersion objective. In SIM, images were captured using a 100x oil immersion objective on a Nikon SIM microscope as previously described [70].

Immunoprecipitation (IP) and immunoblotting

In IP experiments, cells were lysed in IP buffer (25 mM HEPES [pH 7.4], 138 mM NaCl, 10 mM Na3PO4, 2.7 mM KCl, 0.5% CHAPS, 1 mM DTT, and a protease inhibitor cocktail). After centrifugation, proteins were immunoprecipitated from cell extracts using primary antibodies and protein A/G agarose beads (Thermo Scientific, #WF324079). For immunoblotting, immunoprecipitates or whole cell lysates were resolved on 8% Bis-Tris SDS–polyacrylamide gel electrophoresis (SDS-PAGE) and transferred to PVDF membranes. Proteins were detected using unlabeled primary antibodies and horseradish peroxidase (HRP)-conjugated secondary antibodies, or HRP-conjugated primary antibodies. Primary antibodies used in immunoblotting include anti-COMMD3 (Bethyl, #A304-092A, RRID:AB_2621341), anti-VPS35L (Invitrogen, #PA5-28553, RRID: AB_2546029), anti-CCDC93 (Santa Cruz Biotechnology, #sc-514600), anti-alpha-tubulin

(DSHB, #12G10, RRID: AB_1210456), HRP-conjugated anti-FLAG M2 (Sigma-Aldrich, #A8592, RRID: AB_439702), and HRP-conjugated anti-HA (Roche, #12013819001, RRID: AB_390917). Secondary antibodies used in this work include HRP-conjugated anti-rabbit IgG (Sigma-Aldrich, #A6154, RRID: AB_258284) and HRP-conjugated anti-mouse IgG (Sigma-Aldrich, #A6782, RRID: AB_258315). All experiments were run in biological triplicates. Intensities of protein bands on immunoblots were quantified using ImageJ.

Mass spectrometry

Mass spectrometry was carried out as previously described [8]. Immunoprecipitates on protein A/G beads were snap-frozen and stored at -70°C. Peptides were pre-fractionated using high-pH fractionation and analyzed on the Thermo Ultimate 3000 RSLCnano System via direct injection. Data were processed using MaxQuant/Andromeda (version 1.6.2.10) and compared to Uniprot annotated protein sequences. False discovery rates were set to 0.01 for protein and peptide assignment with a minimum peptide length of four residues and a minimum peptide number of one.

Structural prediction and analysis

The structural model of the ARF1-GTP:COMMD3-NTD (a.a. 1-120) heterodimer was predicted using AlphaFold3 with default settings [71]. Five independent structural models were generated for each protein complex, and the quality of the predicted models was assessed through their interface predicted template modeling (ipTM) scores, predicted template modeling (pTM) scores, predicted alignment error (PAE) plots, and predicted local distance difference test (pLDDT) scores

[71, 72]. Structural analysis was conducted using UCSF ChimeraX (v1.8) [73] and PDBePISA [74].

ACKNOWLEDGEMENTS

We thank Drs. Santiago Di Pietro, Da Jia, Andrea Ambrosio, Greg Odorizzi, Gia Voeltz, and Mitchell Leih for reagents or helpful suggestions. We thank Yan Ouyang, Jingyi Wu, James Orth, and Christopher C. Ebmeier for technical assistance. This work was supported by National Institutes of Health grants GM126960 (J.S.) and DK124431 (J.S.).

CONFLICT OF INTEREST

The authors declare that they have no conflicts of interest with the contents of this article.

REFERENCES

1. Bonifacino, J.S. and B.S. Glick, *The mechanisms of vesicle budding and fusion.* Cell, 2004. **116**(2): p. 153-66.
2. Rothman, J.E., *The principle of membrane fusion in the cell (Nobel lecture).* Angew Chem Int Ed Engl, 2014. **53**(47): p. 12676-94.
3. Schekman, R. and P. Novick, *23 genes, 23 years later.* Cell, 2004. **116**(2 Suppl): p. S13-5, 1 p following S19.
4. Bausch-Fluck, D., U. Goldmann, S. Muller, M. van Oostrum, M. Muller, O.T. Schubert, and B. Wollscheid, *The in silico human surfaceome.* Proc Natl Acad Sci U S A, 2018. **115**(46): p. E10988-E10997.
5. Dell'Angelica, E.C. and J.S. Bonifacino, *Coatopathies: Genetic Disorders of Protein Coats.* Annu Rev Cell Dev Biol, 2019. **35**: p. 131-168.
6. Healy, M.D., et al., *Structure of the endosomal Commander complex linked to Ritscher-Schinzel syndrome.* Cell, 2023. **186**(10): p. 2219-2237 e29.
7. Boesch, D.J., A. Singla, Y. Han, D.A. Kramer, Q. Liu, K. Suzuki, P. Juneja, X. Zhao, X. Long, M.J. Medlyn, D.D. Billadeau, Z. Chen, B. Chen, and E. Burstein, *Structural organization of the retriever-CCC endosomal recycling complex.* Nat Struct Mol Biol, 2023.
8. Wang, S., X. Chen, L. Crisman, X. Dou, C.S. Winborn, C. Wan, H. Puscher, Q. Yin, M.J. Kennedy, and J. Shen, *Regulation of cargo exocytosis by a Reps1-Ralbp1-RalA module.* Sci Adv, 2023. **9**(8): p. eade2540.

9. Gulbranson, D.R., L. Crisman, M. Lee, Y. Ouyang, B.L. Menasche, B.A. Demmitt, C. Wan, T. Nomura, Y. Ye, H. Yu, and J. Shen, *AAGAB Controls AP2 Adaptor Assembly in Clathrin-Mediated Endocytosis.* Dev Cell, 2019. **50**(4): p. 436-446 e5.

10. Simonetti, B. and P.J. Cullen, *Actin-dependent endosomal receptor recycling.* Curr Opin Cell Biol, 2019. **56**: p. 22-33.

11. Cullen, P.J. and F. Steinberg, *To degrade or not to degrade: mechanisms and significance of endocytic recycling.* Nat Rev Mol Cell Biol, 2018. **19**(11): p. 679-696.

12. Yong, X., C. Zhou, D.D. Billadeau, and D. Jia, *Commanding the Commander: structure of a key protein machinery in endosomal trafficking.* Signal Transduct Target Ther, 2023. **8**(1): p. 295.

13. Wang, J., A. Fedoseienko, B. Chen, E. Burstein, D. Jia, and D.D. Billadeau, *Endosomal receptor trafficking: Retromer and beyond.* Traffic, 2018. **19**(8): p. 578-590.

14. Ambrosio, A.L., H.P. Febvre, and S.M. Di Pietro, *Syntaxin 12 and COMMD3 are new factors that function with VPS33B in the biogenesis of platelet alpha-granules.* Blood, 2022. **139**(6): p. 922-935.

15. Weeratunga, S., B. Paul, and B.M. Collins, *Recognising the signals for endosomal trafficking.* Curr Opin Cell Biol, 2020. **65**: p. 17-27.

16. Rothman, J.H. and T.H. Stevens, *Protein sorting in yeast: mutants defective in vacuole biogenesis mislocalize vacuolar proteins into the late secretory pathway.* Cell, 1986. **47**(6): p. 1041-51.

17. Bankaitis, V.A., L.M. Johnson, and S.D. Emr, *Isolation of yeast mutants defective in protein targeting to the vacuole.* Proc Natl Acad Sci U S A, 1986. **83**(23): p. 9075-9.

18. Seaman, M.N., J.M. McCaffery, and S.D. Emr, *A membrane coat complex essential for endosome-to-Golgi retrograde transport in yeast.* J Cell Biol, 1998. **142**(3): p. 665-81.

19. Laulumaa, S., E.P. Kumpula, J.T. Huiskonen, and M. Varjosalo, *Structure and interactions of the endogenous human Commander complex.* Nat Struct Mol Biol, 2024.

20. Leneva, N. and O. Kovtun, *The commander complex is the Swiss Army knife of endosomal trafficking.* Nat Struct Mol Biol, 2024. **31**(6): p. 856-858.

21. Mallam, A.L. and E.M. Marcotte, *Systems-wide Studies Uncover Commander, a Multiprotein Complex Essential to Human Development.* Cell Syst, 2017. **4**(5): p. 483-494.

22. McNally, K.E., et al., *Retriever is a multiprotein complex for retromer-independent endosomal cargo recycling.* Nat Cell Biol, 2017. **19**(10): p. 1214-1225.

23. Singla, A., A. Fedoseienko, S.S.P. Giridharan, B.L. Overlee, A. Lopez, D. Jia, J. Song, K. Huff-Hardy, L. Weisman, E. Burstein, and D.D. Billadeau, *Endosomal PI(3)P regulation by the COMMD/CCDC22/CCDC93 (CCC) complex controls membrane protein recycling.* Nat Commun, 2019. **10**(1): p. 4271.

24. van De Sluis, B., J. Rothuizen, P.L. Pearson, B.A. van Oost, and C. Wijmenga, *Identification of a new copper metabolism gene by positional cloning in a purebred dog population.* Hum Mol Genet, 2002. **11**(2): p. 165-73.

25. Burstein, E., J.E. Hoberg, A.S. Wilkinson, J.M. Rumble, R.A. Csomos, C.M. Komarck, G.N. Maine, J.C. Wilkinson, M.W. Mayo, and C.S. Duckett, *COMMD proteins, a novel family of structural and functional homologs of MURR1.* J Biol Chem, 2005. **280**(23): p. 22222-32.

26. Yong, X., L. Zhao, W. Hu, Q. Sun, H. Ham, Z. Liu, J. Ren, Z. Zhang, Y. Zhou, Q. Yang, X. Mo, J. Hu, D.D. Billadeau, and D. Jia, *SNX27-FERM-SNX1 complex structure rationalizes divergent trafficking pathways by SNX17 and SNX27.* Proc Natl Acad Sci U S A, 2021. **118**(36).

27. Uhlen, M., et al., *Proteomics. Tissue-based map of the human proteome.* Science, 2015. **347**(6220): p. 1260419.

28. You, G., C. Zhou, L. Wang, Z. Liu, H. Fang, X. Yao, and X. Zhang, *COMMD proteins function and their regulating roles in tumors.* Front Oncol, 2023. **13**: p. 1067234.

29. Healy, M.D., M.K. Hospenthal, R.J. Hall, M. Chandra, M. Chilton, V. Tillu, K.E. Chen, D.J. Celligoi, F.J. McDonald, P.J. Cullen, J.S. Lott, B.M. Collins, and R. Ghai, *Structural insights into the architecture and membrane interactions of the conserved COMMD proteins.* Elife, 2018. **7**.

30. Shirai, T., et al., *Celastrol suppresses humoral immune responses and autoimmunity by targeting the COMMD3/8 complex.* Sci Immunol, 2023. **8**(81): p. eadc9324.

31. Nakai, A., J. Fujimoto, H. Miyata, R. Stumm, M. Narazaki, S. Schulz, Y. Baba, A. Kumanogoh, and K. Suzuki, *The COMMD3/8 complex determines GRK6 specificity for chemoattractant receptors.* J Exp Med, 2019. **216**(7): p. 1630-1647.

32. Campion, C.G., K. Zaoui, T. Verissimo, S. Cossette, H. Matsuda, N. Solban, P. Hamet, and J. Tremblay, *COMMD5/HCaRG Hooks Endosomes on Cytoskeleton and Coordinates EGFR Trafficking.* Cell Rep, 2018. **24**(3): p. 670-684 e7.

33. Suraweera, A., N.S. Gandhi, S. Beard, J.T. Burgess, L.V. Croft, E. Bolderson, A. Naqi, N.W. Ashton, M.N. Adams, K.I. Savage, S.D. Zhang, K.J. O'Byrne, and D.J. Richard,

COMMD4 functions with the histone H2A-H2B dimer for the timely repair of DNA double-strand breaks. Commun Biol, 2021. **4**(1): p. 484.

34. Gulbranson, D.R., E.M. Davis, B.A. Demmitt, Y. Ouyang, Y. Ye, H. Yu, and J. Shen, *RABIF/MSS4 is a Rab-stabilizing holdase chaperone required for GLUT4 exocytosis.* Proc Natl Acad Sci U S A, 2017. **114(39)**: p. E8224-E8233.
35. Ran, F.A., P.D. Hsu, J. Wright, V. Agarwala, D.A. Scott, and F. Zhang, *Genome engineering using the CRISPR-Cas9 system.* Nat Protoc, 2013. **8**(11): p. 2281-308.
36. Pan, X., N. Zaarur, M. Singh, P. Morin, and K.V. Kandror, *Sortilin and retromer mediate retrograde transport of Glut4 in 3T3-L1 adipocytes.* Molecular biology of the cell, 2017. **28**(12): p. 1667-1675.
37. Ahfeldt, T., et al., *Programming human pluripotent stem cells into white and brown adipocytes.* Nat Cell Biol, 2012. **14**(2): p. 209-19.
38. Mishra, A., S. Eathiraj, S. Corvera, and D.G. Lambright, *Structural basis for Rab GTPase recognition and endosome tethering by the C2H2 zinc finger of Early Endosomal Autoantigen 1 (EEA1).* Proc Natl Acad Sci U S A, 2010. **107**(24): p. 10866-71.
39. Langemeyer, L., F. Frohlich, and C. Ungermann, *Rab GTPase Function in Endosome and Lysosome Biogenesis.* Trends Cell Biol, 2018. **28**(11): p. 957-970.
40. Puthenveedu, M.A., B. Lauffer, P. Temkin, R. Vistein, P. Carlton, K. Thorn, J. Taunton, O.D. Weiner, R.G. Parton, and M. von Zastrow, *Sequence-dependent sorting of recycling proteins by actin-stabilized endosomal microdomains.* Cell, 2010. **143**(5): p. 761-73.
41. Maine, G.N. and E. Burstein, *COMMD proteins: COMMing to the scene.* Cell Mol Life Sci, 2007. **64**(15): p. 1997-2005.

42. Nakai, W., Y. Kondo, A. Saitoh, T. Naito, K. Nakayama, and H.W. Shin, *ARF1 and ARF4 regulate recycling endosomal morphology and retrograde transport from endosomes to the Golgi apparatus.* Mol Biol Cell, 2013. **24**(16): p. 2570-81.

43. Stockhammer, A., et al., *ARF1 compartments direct cargo flow via maturation into recycling endosomes.* Nat Cell Biol, 2024.

44. D'Souza-Schorey, C. and P. Chavrier, *ARF proteins: roles in membrane traffic and beyond.* Nat Rev Mol Cell Biol, 2006. **7**(5): p. 347-58.

45. Goldberg, J., *Structural basis for activation of ARF GTPase: mechanisms of guanine nucleotide exchange and GTP-myristoyl switching.* Cell, 1998. **95**(2): p. 237-48.

46. Sauvageau, E., P.J. McCormick, and S. Lefrancois, *In vivo monitoring of the recruitment and activation of AP-1 by Arf1.* Sci Rep, 2017. **7**(1): p. 7148.

47. Menasche, B.L., E.M. Davis, S. Wang, Y. Ouyang, S. Li, H. Yu, and J. Shen, *PBRM1 and the glycosylphosphatidylinositol biosynthetic pathway promote tumor killing mediated by MHC-unrestricted cytotoxic lymphocytes.* Sci Adv, 2020. **6**(48).

48. Davis, E.M., J. Kim, B.L. Menasche, J. Sheppard, X. Liu, A.C. Tan, and J. Shen, *Comparative Haploid Genetic Screens Reveal Divergent Pathways in the Biogenesis and Trafficking of Glycophosphatidylinositol-Anchored Proteins.* Cell Rep, 2015. **11**(11): p. 1727-36.

49. Kondo, Y., A. Hanai, W. Nakai, Y. Katoh, K. Nakayama, and H.W. Shin, *ARF1 and ARF3 are required for the integrity of recycling endosomes and the recycling pathway.* Cell Struct Funct, 2012. **37**(2): p. 141-54.

50. Li, H., Y. Koo, X. Mao, L. Sifuentes-Dominguez, L.L. Morris, D. Jia, N. Miyata, R.A. Faulkner, J.M. van Deursen, M. Vooijs, D.D. Billadeau, B. van de Sluis, O. Cleaver, and

E. Burstein, *Endosomal sorting of Notch receptors through COMMD9-dependent pathways modulates Notch signaling.* J Cell Biol, 2015. **211**(3): p. 605-17.

51. Bartuzi, P., M.H. Hofker, and B. van de Sluis, *Tuning NF-kappaB activity: a touch of COMMD proteins.* Biochim Biophys Acta, 2013. **1832**(12): p. 2315-21.

52. Esposito, E., G. Napolitano, A. Pescatore, G. Calculli, M.R. Incoronato, A. Leonardi, and M.V. Ursini, *COMMD7 as a novel NEMO interacting protein involved in the termination of NF-kappaB signaling.* J Cell Physiol, 2016. **231**(1): p. 152-61.

53. O'Hara, A., J. Simpson, P. Morin, C.J. Loveridge, A.C. Williams, S.M. Novo, and L.A. Stark, *p300-mediated acetylation of COMMD1 regulates its stability, and the ubiquitylation and nucleolar translocation of the RelA NF-kappaB subunit.* J Cell Sci, 2014. **127**(Pt 17): p. 3659-65.

54. Riera-Romo, M., *COMMD1: A Multifunctional Regulatory Protein.* J Cell Biochem, 2018. **119**(1): p. 34-51.

55. You, N., J. Li, X. Huang, K. Wu, Y. Tang, L. Wang, H. Li, N. Mi, and L. Zheng, *COMMD7 activates CXCL10 production by regulating NF-kappaB and the production of reactive oxygen species.* Mol Med Rep, 2018. **17**(5): p. 6784-6788.

56. Mao, X., N. Gluck, B. Chen, P. Starokadomskyy, H. Li, G.N. Maine, and E. Burstein, *COMMD1 (copper metabolism MURR1 domain-containing protein 1) regulates Cullin RING ligases by preventing CAND1 (Cullin-associated Nedd8-dissociated protein 1) binding.* J Biol Chem, 2011. **286**(37): p. 32355-65.

57. de Bie, P., B. van de Sluis, E. Burstein, K.J. Duran, R. Berger, C.S. Duckett, C. Wijmenga, and L.W. Klomp, *Characterization of COMMD protein-protein interactions in NF-kappaB signalling.* Biochem J, 2006. **398**(1): p. 63-71.

58. Maine, G.N., X. Mao, C.M. Komarck, and E. Burstein, *COMMD1 promotes the ubiquitination of NF-kappaB subunits through a cullin-containing ubiquitin ligase.* EMBO J, 2007. **26**(2): p. 436-47.

59. Phillips-Krawczak, C.A., et al., *COMMD1 is linked to the WASH complex and regulates endosomal trafficking of the copper transporter ATP7A.* Mol Biol Cell, 2015. **26**(1): p. 91-103.

60. Bartuzi, P., et al., *CCC- and WASH-mediated endosomal sorting of LDLR is required for normal clearance of circulating LDL.* Nat Commun, 2016. **7**: p. 10961.

61. Hancock, J.L., M. Kalimutho, J. Straube, M. Lim, I. Gresshoff, J.M. Saunus, J.S. Lee, S.R. Lakhani, K.J. Simpson, A.I. Bush, R.L. Anderson, and K.K. Khanna, *COMMD3 loss drives invasive breast cancer growth by modulating copper homeostasis.* J Exp Clin Cancer Res, 2023. **42**(1): p. 90.

62. Liu, Y.F., M. Swart, Y. Ke, K. Ly, and F.J. McDonald, *Functional interaction of COMMD3 and COMMD9 with the epithelial sodium channel.* Am J Physiol Renal Physiol, 2013. **305**(1): p. F80-9.

63. Weiskirchen, R. and L.C. Penning, *COMMD1, a multi-potent intracellular protein involved in copper homeostasis, protein trafficking, inflammation, and cancer.* J Trace Elem Med Biol, 2021. **65**: p. 126712.

64. Jiang, Z., W. Chen, J. Zhou, Q. Peng, H. Zheng, Y. Yuan, H. Cui, W. Zhao, X. Sun, Z. Zhou, and X. Liu, *Identification of COMMD1 as a novel lamin A binding partner.* Mol Med Rep, 2019. **20**(2): p. 1790-1796.

65. Dumoulin, B., C. Ufer, S. Stehling, D. Heydeck, H. Kuhn, and S. Sofi, *Identification of the COMM-domain containing protein 1 as specific binding partner for the guanine-rich*

RNA sequence binding factor 1. Biochim Biophys Acta Gen Subj, 2020. **1864**(11): p. 129678.

66. Liebeskind, B.J., R.W. Aldrich, and E.M. Marcotte, *Ancestral reconstruction of protein interaction networks.* PLoS Comput Biol, 2019. **15**(10): p. e1007396.

67. Yang, M., W. Huang, Y. Sun, H. Liang, M. Chen, X. Wu, X. Wang, L. Zhang, X. Cheng, Y. Fan, H. Pan, L. Chen, and J. Guan, *Prognosis and modulation mechanisms of COMMD6 in human tumours based on expression profiling and comprehensive bioinformatics analysis.* Br J Cancer, 2019. **121**(8): p. 699-709.

68. Niu, X., J. Hong, X. Zheng, D.B. Melville, E.W. Knapik, A. Meng, and J. Peng, *The nuclear pore complex function of Sec13 protein is required for cell survival during retinal development.* J Biol Chem, 2014. **289**(17): p. 11971-11985.

69. Enninga, J., A. Levay, and B.M. Fontoura, *Sec13 shuttles between the nucleus and the cytoplasm and stably interacts with Nup96 at the nuclear pore complex.* Mol Cell Biol, 2003. **23**(20): p. 7271-84.

70. Wan, C., H. Puscher, Y. Ouyang, J. Wu, Y. Tian, S. Li, Q. Yin, and J. Shen, *An AAGAB-to-CCDC32 handover mechanism controls the assembly of the AP2 adaptor complex.* Proc Natl Acad Sci U S A, 2024. **121**(34): p. e2409341121.

71. Abramson, J., et al., *Accurate structure prediction of biomolecular interactions with AlphaFold 3.* Nature, 2024. **630**(8016): p. 493-500.

72. Mirdita, M., K. Schutze, Y. Moriwaki, L. Heo, S. Ovchinnikov, and M. Steinegger, *ColabFold: making protein folding accessible to all.* Nat Methods, 2022. **19**(6): p. 679-682.

73. Goddard, T.D., C.C. Huang, E.C. Meng, E.F. Pettersen, G.S. Couch, J.H. Morris, and T.E. Ferrin, *UCSF ChimeraX: Meeting modern challenges in visualization and analysis.* Protein Sci, 2018. **27**(1): p. 14-25.

74. Krissinel, E. and K. Henrick, *Inference of macromolecular assemblies from crystalline state.* J Mol Biol, 2007. **372**(3): p. 774-97.

75. Klip, A., T.E. McGraw, and D.E. James, *Thirty sweet years of GLUT4.* J Biol Chem, 2019. **294**(30): p. 11369-11381.

76. Blot, V. and T.E. McGraw, *Use of quantitative immunofluorescence microscopy to study intracellular trafficking: studies of the GLUT4 glucose transporter.* Methods Mol Biol, 2008. **457**: p. 347-66.

77. Cohen, L.A. and J.G. Donaldson, *Analysis of Arf GTP-binding protein function in cells.* Curr Protoc Cell Biol, 2010. **Chapter 3**: p. Unit 14 12 1-17.

78. Zhang, C.J., A.G. Rosenwald, M.C. Willingham, S. Skuntz, J. Clark, and R.A. Kahn, *Expression of a dominant allele of human ARF1 inhibits membrane traffic in vivo.* J Cell Biol, 1994. **124**(3): p. 289-300.

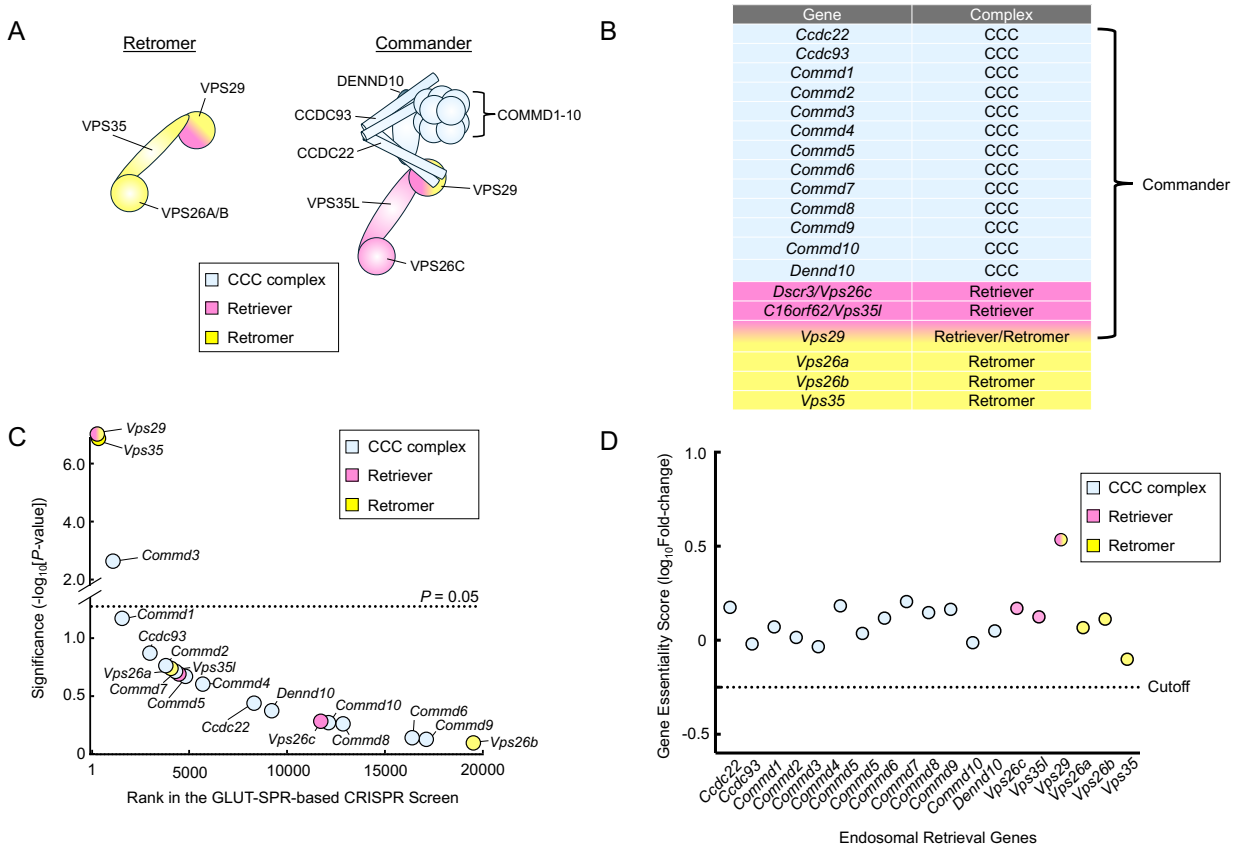

Figure 1. Genetic analysis of genes encoding Retromer and Commander subunits using unbiased genome-wide CRISPR screens. (A) Cartoon representation of the Retromer and Commander complexes. **(B)** Table listing genes encoding the subunits of the Retromer and Commander complexes. **(C)** Ranking of genes encoding the Retromer and Commander complexes in an unbiased CRISPR screen that was conducted to identify genes required for the surface homeostasis of GLUT-SPR [8]. The GLUT-SPR reporter was constructed by inserting a hemagglutinin (HA) epitope into an exoplasmic loop of the glucose transporter GLUT4, with a GFP tag fused to the intracellular C-terminus of GLUT4 [34, 75, 76]. Surface expression (HA staining) of the reporter was normalized to total reporter expression (GFP fluorescence) as a measure of relative surface levels of the reporter. Each dot represents a gene. The dashed line depicts the *P*-value cutoff at 0.05. **(D)** Essentiality scores of genes encoding the Retromer and

Commander complexes calculated by comparing gRNA abundance in a passage cell population (without any selection) with that in the initial CRISPR library. Genes with essentiality scores below the horizontal cutoff line are predicted to be essential to cell survival or growth. Full datasets of the CRISPR screens are included in a previous report [8].

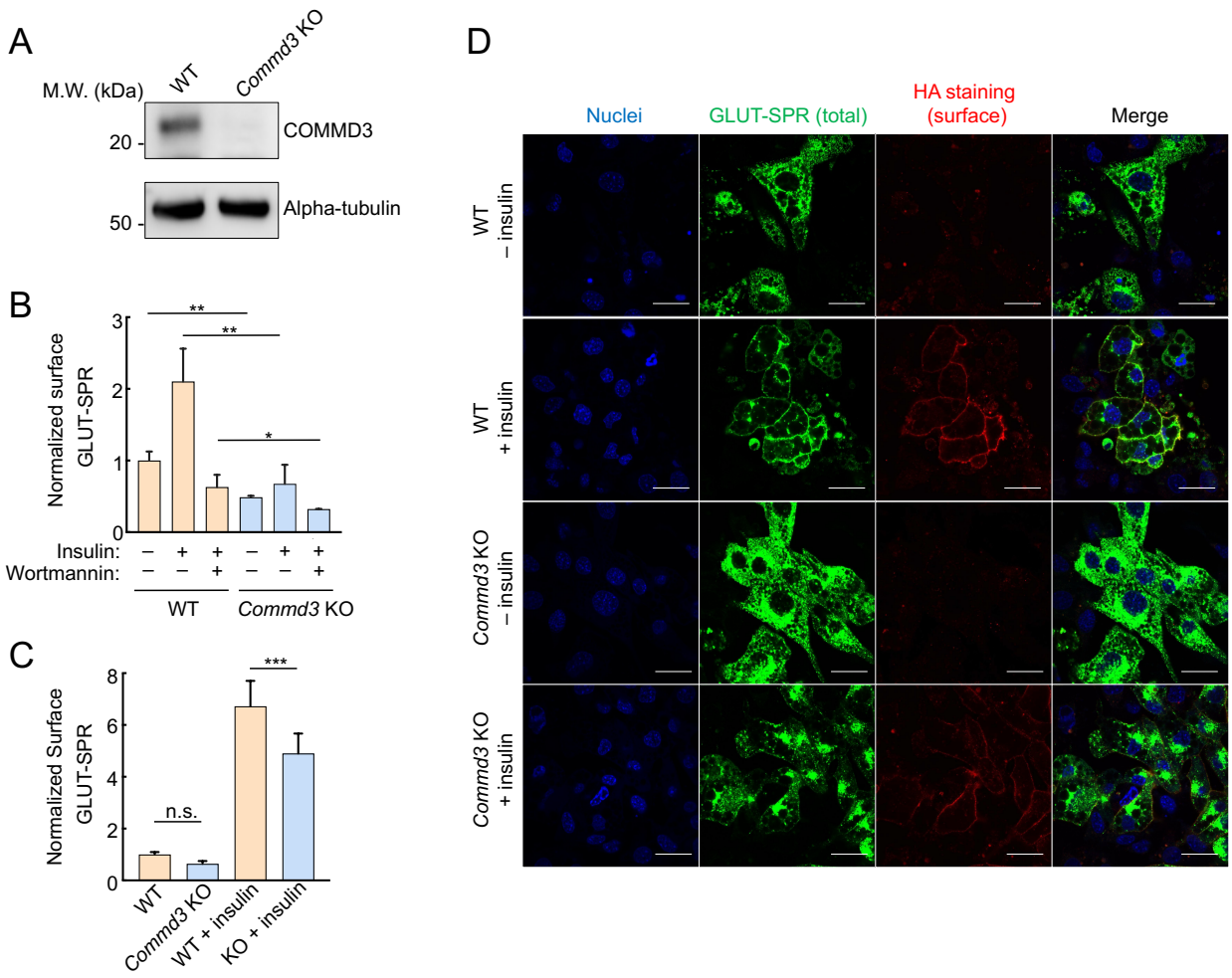

Figure 2. Intracellular sequestration of GLUT-SPR in COMMD3-deficient cells. (A) Representative immunoblots showing the indicated proteins in wild-type (WT) and *Commd3* KO mouse preadipocytes. **(B)** Normalized surface levels of GLUT-SPR measured by flow cytometry in WT and KO preadipocytes. The cells were either untreated or treated with 100 nM insulin for one hour before surface GLUT-SPR was labeled using anti-HA antibodies and APC-conjugated secondary antibodies. To inhibit insulin signaling, 100 nM wortmannin was added prior to insulin stimulation. In all figures, data normalization was performed by setting the mean value of WT data points as 100 or 1, and all data points including WT ones were normalized to that mean value. Data are presented as mean ± SD of three biological replicates. ** $P < 0.01$; * $P < 0.05$ (calculated

using Student's t-test). **(C)** Normalized surface levels of GLUT-SPR in WT and KO adipocytes. Data are presented as mean ± SD of three biological replicates. *** $P < 0.001$; n.s., $P > 0.05$ (calculated using Student's t-test). **(D)** Representative confocal images showing the localization of GLUT-SPR in unpermeabilized WT and *Commd3* KO adipocytes, which were either untreated or treated with 100 nM insulin for one hour. Surface GLUT-SPR was labeled using anti-HA antibodies and Alexa Fluor 568-conjugated secondary antibodies. Nuclei were stained with Hoechst 33342. Scale bars: 10 μm.

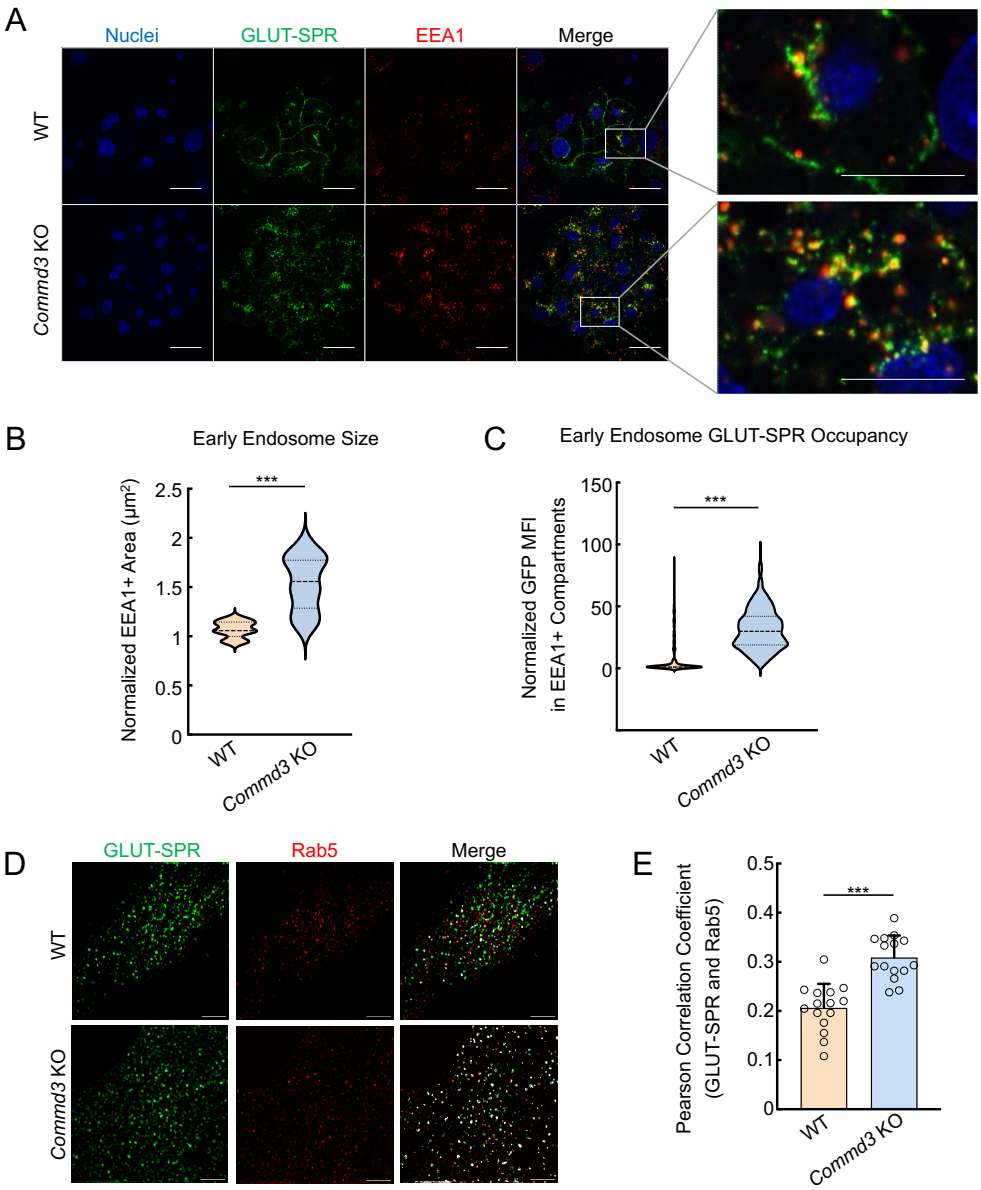

Figure 3. Abnormal endosomal morphology in COMMD3-deficient cells. (A) Representative confocal images showing the localization of EEA1 and GLUT-SPR in permeabilized WT and *Commd3* KO adipocytes stimulated with 100 nM insulin for one hour (scale bars: 10 μm). Enlarged inset images depict co-localization of EEA1 and GLUT-SPR (scale bars: 5 μm). **(B)** Violin plot showing quantification of EEA1-positive puncta using Fiji threshold analysis. Data of the KO adipocytes were normalized to those of WT cells. Three independent experiments are shown with

ten cells analyzed in each experiment. *** $P < 0.001$ (calculated using Student's t-test). **(C)** Violin plot depicting quantification of GFP mean fluorescence intensity (MFI) in EEA1-positive puncta using Fiji threshold analysis. Data of KO adipocytes were normalized to those of WT cells. Three independent experiments are shown with ten cells analyzed in each experiment. *** $P < 0.001$ (calculated using Student's t-test). **(D)** Representative SIM images showing the subcellular localization of Rab5 and GLUT-SPR in WT and *Commd3* KO preadipocytes (scale bars: 5 μm). **(E)** Quantification of Rab5 and GLUT-SPR co-localization based on SIM images, which were captured as in (D) and analyzed using ImageJ. Each dot represents data of a subcellular region of interest. Five cells were analyzed and three regions per cell were quantified. *** $P < 0.001$ (calculated using Student's t-test).

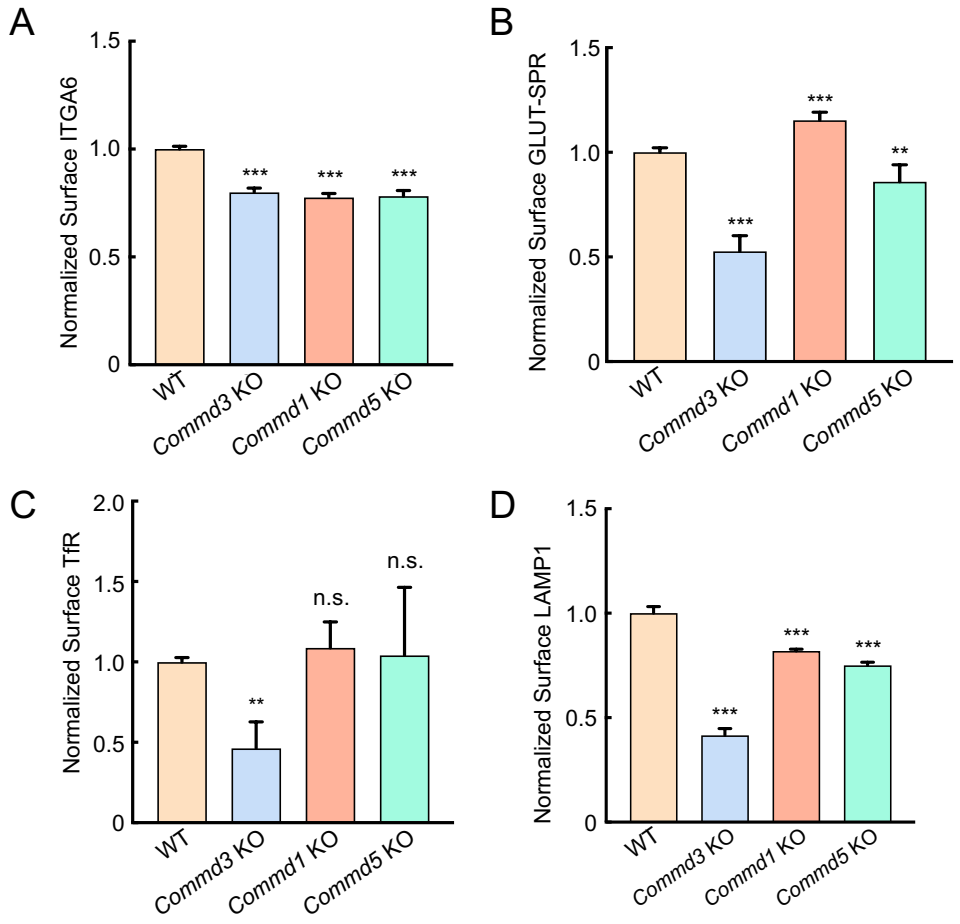

Figure 4. COMMD3 regulates a group of cargo proteins independent of other COMMD proteins. (A-D) Normalized surface levels of ITGA6 (A), GLUT-SPR (B), TfR (C) and LAMP1 (D) measured by flow cytometry in the indicated preadipocyte cell lines. Data of all cell samples were normalized to those of WT cells. Data of ITGA6 (n=3), GLUT-SPR (n=6), TfR (n=10) and LAMP1 (n=3) are presented as mean ± SD. ** $P < 0.01$; *** $P < 0.001$; n.s., $P > 0.05$ (calculated using one-way ANOVA).

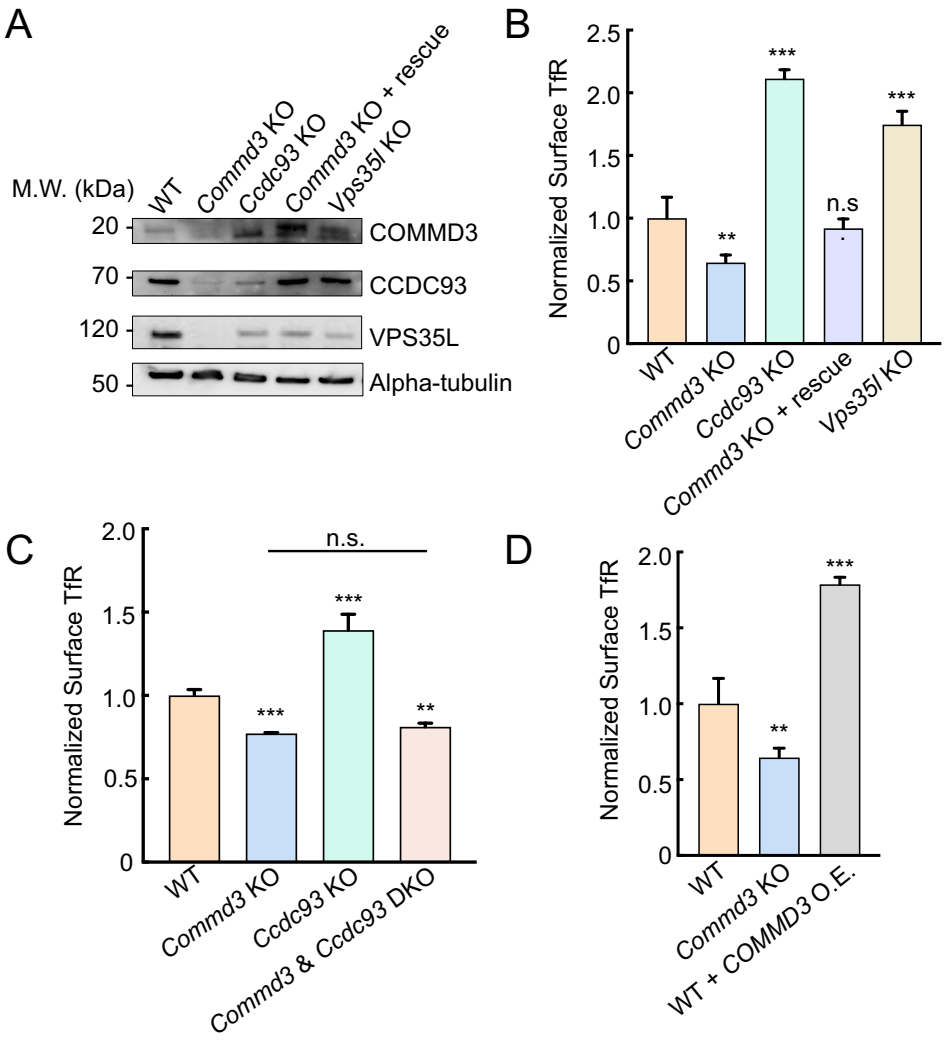

Figure 5. Upregulation of COMMD3 in cells deficient in CCDC93 or VPS35L. (A) Representative immunoblots showing protein expression in the indicated preadipocyte cell lines. **(B-D)** Normalized surface levels of TfR measured by flow cytometry in the indicated preadipocyte cell lines. Data of all cell samples were normalized to those of WT cells. Data are presented as mean ± SD of three biological replicates. ** $P < 0.01$; *** $P < 0.001$; n.s., $P > 0.05$ (calculated using one-way ANOVA).

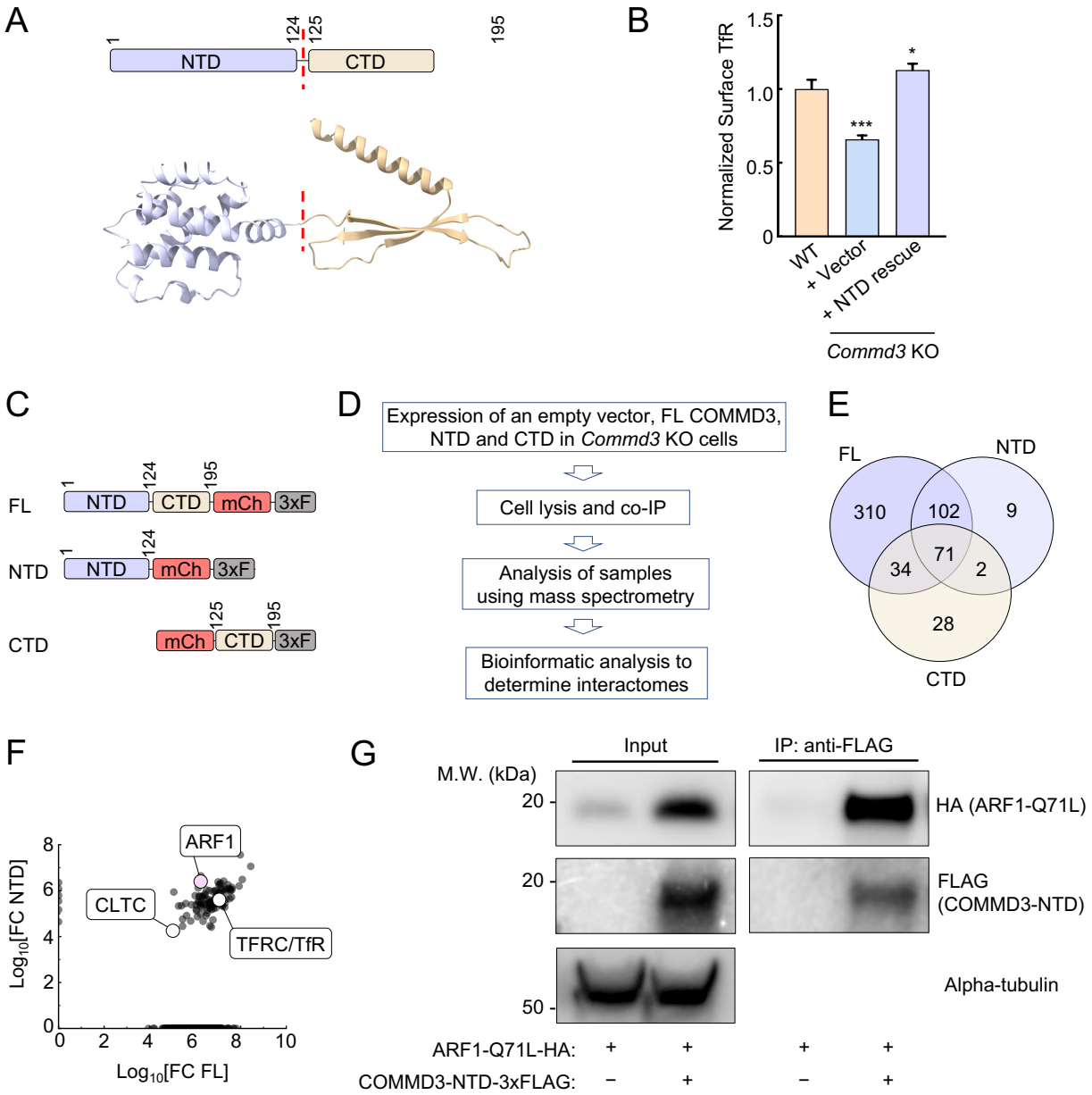

Figure 6. The Commander-independent function of COMMD3 is mediated by its NTD. (A) Top, diagram depicting the domain organization of COMMD3. Bottom: the structural model of COMMD3 (AlphaFold Protein Structure Database: AF-Q9UBI1-F1) showing the independently folded NTD and CTD. **(B)** Normalized surface levels of TfR measured by flow cytometry in the indicated preadipocyte cell lines. Data of all cell samples were normalized to those of WT cells. Data are presented as mean ± SD of three biological replicates. * $P < 0.05$; *** $P < 0.001$

(calculated using one-way ANOVA). **(C)** Diagrams of FL and truncated COMMD3 proteins used in proteomic experiments. The proteins were tagged with mCherry (mCh) and 3xFLAG (3xF). **(D)** Procedures of proteomic analysis to determine the interactomes of FL and truncated COMMD3 proteins. **(E)** Venn diagram showing the interactomes of COMMD3 proteins. **(F)** A scatter plot showing the fold-change of protein abundance over vector control in the interactomes of FL COMMD3 and the NTD of COMMD3. Selected proteins are labeled. **(G)** Representative immunoblots showing the interactions of ARF1 Q71L with COMMD3-NTD. HA-tagged ARF1 Q71L and 3xFLAG-tagged COMMD3-NTD were co-expressed in 293T cells. COMMD3-NTD and associated proteins were immunoprecipitated using anti-FLAG antibodies and detected using immunoblotting. The ARF Q71L mutant was used here because it adopts a GTP-bound configuration [77, 78].

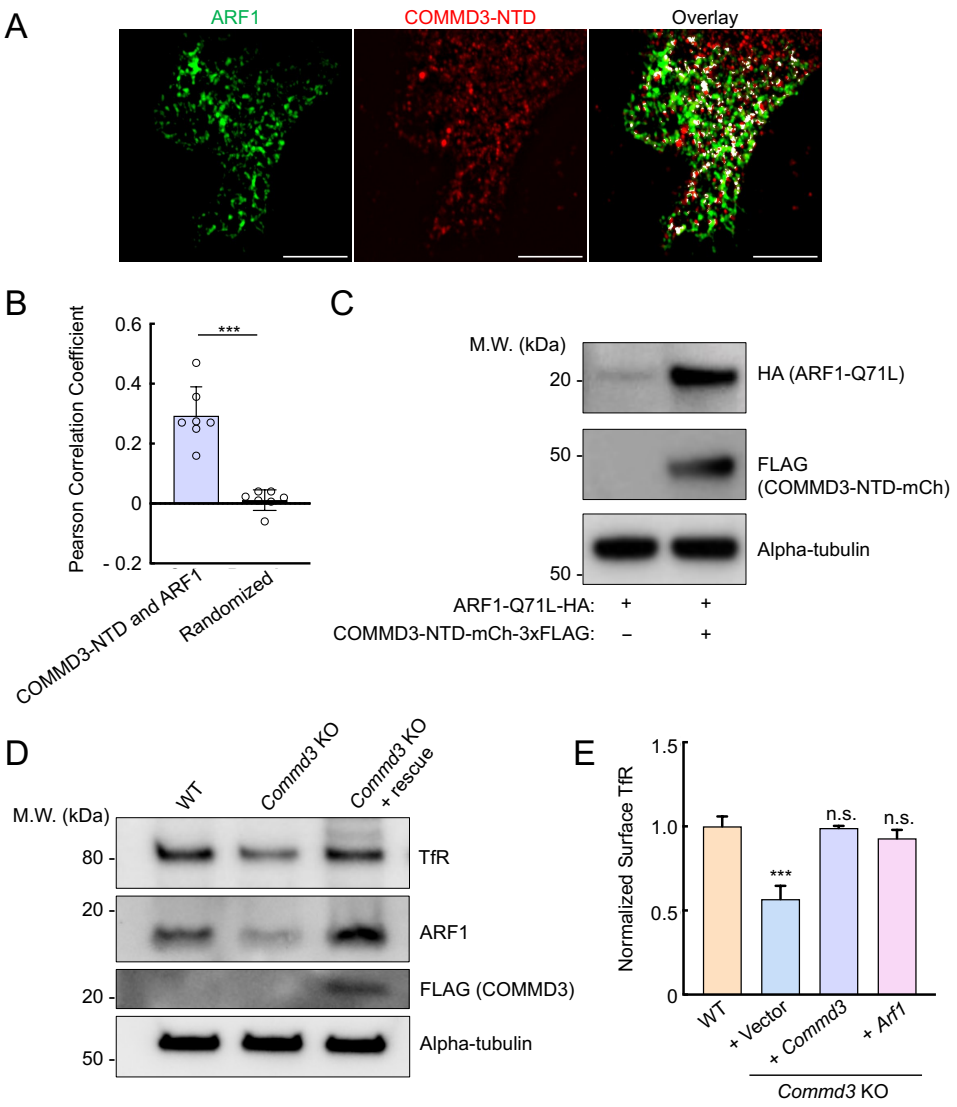

Figure 7. The NTD of COMMD3 stabilizes ARF1. (A) Representative SIM images showing the subcellular localization of ARF1 and COMMD3-NTD expressed in HeLa cells. HA-tagged ARF1 and 3xFLAG-tagged COMMD3-NTD were transiently expressed in HeLa cells and stained using anti-HA and anti-FLAG antibodies, respectively (scale bars: 5 µm). **(B)** Quantification of ARF1 and COMMD3-NTD co-localization based on SIM images, which were captured as in (A) and analyzed using ImageJ. Each dot represents data of an individual cell. In randomized samples, ARF1 images were rotated 90° clockwise, whereas COMMD3-NTD images were not rotated. *** $P < 0.001$ (calculated using Student's t-test). **(C)** Representative immunoblots showing the

ARF1-stabilizing effects of COMMD3-NTD. HA-tagged ARF1 Q71L and 3xFLAG-tagged COMMD3-NTD were transiently expressed in HeLa cells and their total expression levels were measured using immunoblotting. **(D)** Representative immunoblots showing protein expression in the indicated preadipocyte cell lines. **(E)** Normalized surface levels of TfR measured by flow cytometry in the indicated preadipocyte cell lines. Data of all cell samples were normalized to those of WT preadipocytes. Data are presented as mean ± SD of three biological replicates. *** $P < 0.001$; n.s., $P > 0.05$ (calculated using one-way ANOVA).

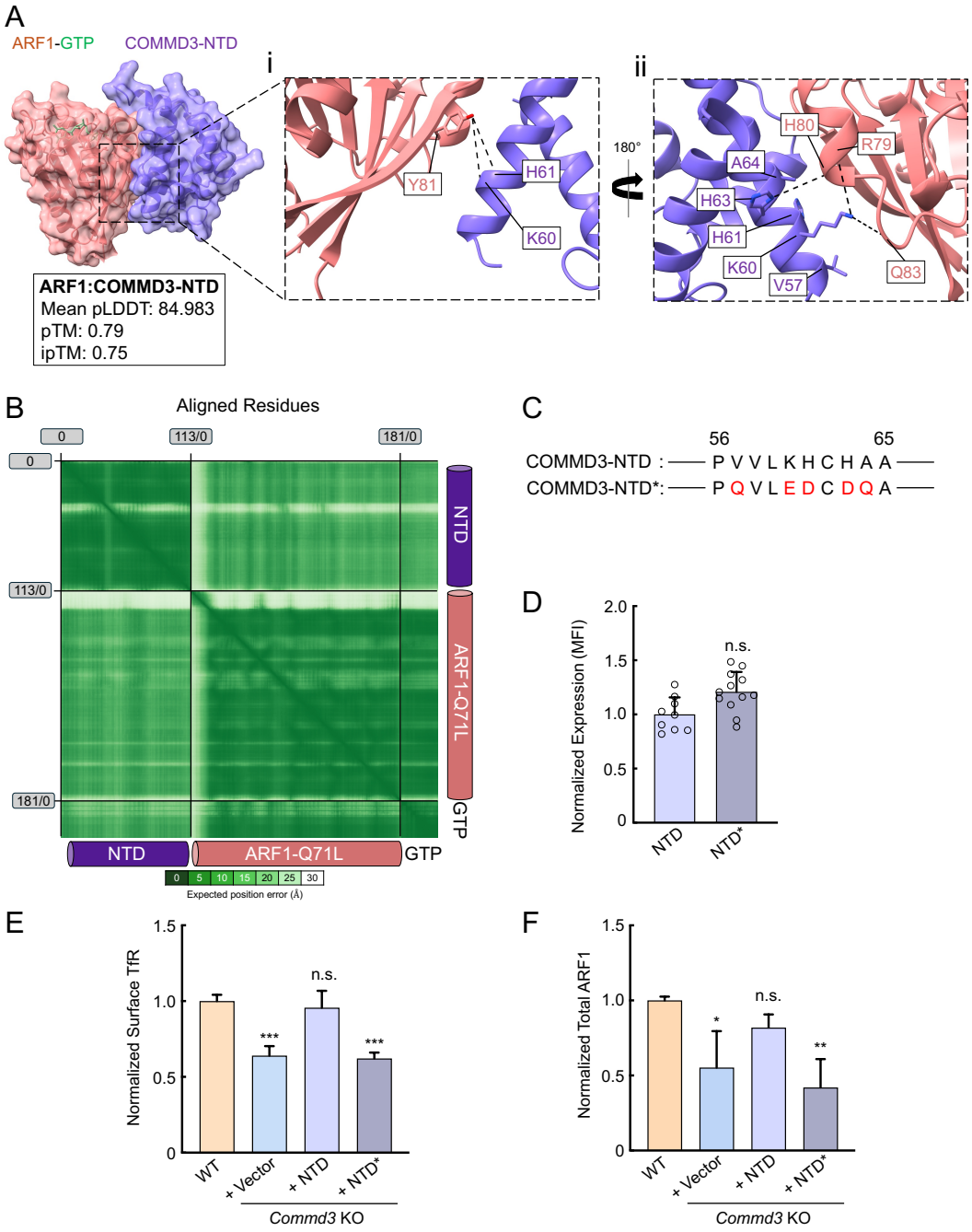

Figure 8. The COMMD3-ARF1 interaction is critical to the Commander-independent function of COMMD3. (A) Left: the AlphaFold3-predicted structure of the COMMD3:ARF1 heterodimer visualized using ChimeraX1.8. The structural prediction was performed using COMMD3-NTD (a.a. 1-120, purple), ARF1 (pink), and GTP (green) as input. Right: key residues

at the COMMD3-ARF1 binding interface. The CIF file of the structural model is included in Supplementary Dataset 1. **(B)** PAE heatmap of the structural model shown in (A). **(C)** Diagrams showing the residues mutated in a COMMD3-NTD mutant (COMMD3-NTD*, only a.a. 56-65 are shown). Mutated residues are shown in red. **(D)** Quantification of COMMD-NTD and NTD* stably expressed in preadipocytes based on SIM images, which were captured and analyzed as in Fig. 7A-B. Each dot represents data of an individual cell. MFI, mean fluorescence intensity. n.s., $P > 0.05$ (calculated using Student's t-test). **(E)** Normalized surface levels of TfR measured by flow cytometry in the indicated preadipocyte cell lines. Data of all cell samples were normalized to those of WT cells. Data are presented as mean ± SD of three biological replicates. *** $P < 0.001$; n.s., $P > 0.05$ (calculated using one-way ANOVA). **(F)** Quantification of endogenous ARF1 in the indicated preadipocyte cell lines based on intensities of proteins on immunoblots quantified using ImageJ. Data of all samples were normalized to those of WT cells. Data are presented as mean ± SD of three biological replicates. * $P < 0.05$; n.s., $P > 0.05$; ** $P < 0.01$ (calculated using one-way ANOVA).

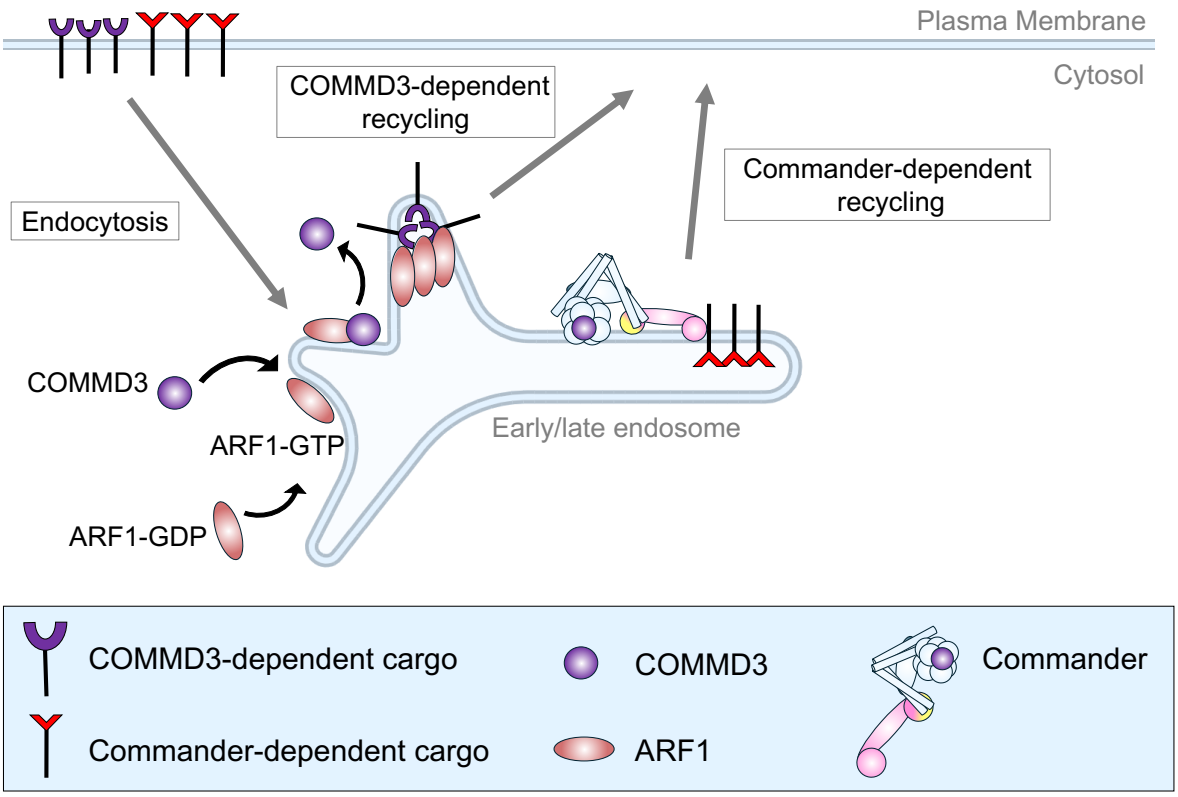

Figure 9. Model of the Commander-independent function of COMMD3 in endosomal trafficking. For clarity, Retromer and other endosomal recycling regulators are not shown.